Preparation and scanning probe microscopic characterization of monolayers of ligand-stabilized transition metal clusters and colloids

Günter Schmid* and Stefanie Peschel

Institut für Anorganische Chemie, Universität Essen, Universitätsstrasse 5–7, D-45117 Essen, Germany

The two-dimensional arrangement of ligand-stabilized transition metal colloids and clusters is of great interest with regard to their electronic properties, possibly exhibiting quantum mechanical effects. According to the principle of self-assembly, colloid and cluster monolayers can be prepared on suitable supports by a simple dipping process. Mica sheets and tempered gold films offer relatively smooth surfaces on which the metal particles have the chance to adsorb in a dense and regular manner. The success of the self-organization of the molecules on the substrates in itself, as well as the density of packing and order of their monolayers, can be verified with surface sensitive physical methods such as scanning tunneling microscopy and scanning force microscopy. The interpretation of the microscopic images of the self-assembled monolayers is facilitated by comparing them with previous microscopic measurements on pure colloids and clusters densely packed within and on the surfaces of their pellets.

Préparation et characterisation par microscopie à champ moche à balayage de monocouches d'agrégats et de colloïds de métaux de transition stabilisés par des ligands. Les arrangements en deux dimensions de colloïdes et agrégats composés de métaux de transition et stabilisés par des ligands sont d'un grand intérêt en raison de leurs propriétés électroniques qui peuvent éventuellement présenter des effets de taille quantique. Selon les principes d'auto-assemblage, des monocouches de colloïdes et agrégats peuvent être préparées sur des supports appropriés par des simples procédés d'immersion. Des films d'or traités thermiquement ainsi que des feuilles de mica présentant des surfaces relativement lisses, les particules métalliques ont la possibilité d'y être adsorbées de façon dense et régulière. La réussite de cette auto-organisation des molécules sur le support ainsi que leur densité d'implantation et la régularité des monocouches peuvent être contrôlées par l'utilisation de méthodes physiques d'études de surface (microscopie à effet tunnel à balayage ou microscopie à force atomique). L'interprétation des images microscopiques de ces monocouches est facilitée après comparaison avec des mesures réalisées en surface de pastilles de colloïdes et agrégats purs.

In addition to their well-known catalytic properties,[1–3] ligand-stabilized clusters and colloids of a size in the nanometer range also exhibit quantum mechanical properties that make them promising candidates for application in nanotechnology and microelectronics.[1,2,4–7] Due to the reduction of the dimensionality of a metal particle the typical metallic properties vanish and quantum size effects appear as a consequence of the quantum confinement of the valence electrons parallel to the reduced dimension.[1,2,5,8–11] The more the dimensionality is reduced the more the electronic density of states decreases and the more the electronic energy levels of the formerly quasi-continuous band structure split.[8] Nimtz and Marquardt[12] described this behaviour as a size-induced metal insulator transition (SIMIT) effect, experimentally seen by a decreasing conductivity of the metal particles with decreasing size.

In consequence the electronic, optical and quantum mechanical properties of a material are adjustable by controlling its dimensionality.[1,8,9,13,14] So, small metal particles can be used in the field of electronics based on the quantum mechanical tunneling of single electrons (SET effect) through a tunneling contact.[4,14,15] With the miniaturization of a contact the temperature at which the SET effect is observable can be drastically elevated. Simon and colleagues[5,11] were able to detect the tunneling of single electrons at room temperature between a pair of ligand-stabilized $Au_{55}(PPh_3)_{12}Cl_6$ clusters.[16,17] In analogy to the construction of a tunneling contact, the ligand shells between the metal cores served as an insulating tunneling barrier through which tunneling could occur.

Monomolecular layers of ligand-stabilized clusters and colloids build up a two-dimensional network of a high number of parallel working tunneling contacts, with each particle acting as a microelectrode. Due to the reduced dimensionality they offer the possibility of measuring the lateral conductivity of the ideally closest packed and regular two-dimensional arrangement of the particles. The examination of the conductivity of a single particle lying on a conductive substrate is also possible by probing it vertically. In both cases the electronic properties may deviate from the semiconductor behaviour,[11,18] especially for ligand-stabilized clusters in a three-dimensional and densely packed arrangement as in pellets, and may exhibit quantum size effects.

According to the principle of self-assembly, the investigated monolayers of clusters and colloids are prepared by dipping a qualified support into a solution of the adsorbing species.[19] Depending on the dipping time the adsorbing molecules have the opportunity to arrange in a regular and dense manner. Often, the substrate first has to be modified by self-assembling a monolayer of mostly organic spacer molecules, in order to be able to react physically or chemically with the clusters and colloids in a following adsorption step. Scanning tunneling microscopy (STM) and atomic force microscopy (AFM)[20–22] are the most suitable physical and surface sensitive methods to judge the surface roughness of the supports and to verify the success of the monolayer preparation. Both scanning methods give information on the electronic and topographic features of an examined surface.

AFM monitors the total electron density distribution of the

scanned surface, which can be correlated with the surface topography, whereas STM reflects the partial electron density distribution in the vicinity of the Fermi level of the examined conductive or semiconductive surface.[21] STM images can be correlated with the substrate topography only if its surface is homogeneous. Inhomogenities make the interpretation of the STM images difficult and requires special information on the local electronic structures.[21,23] The layers of ligand-stabilized clusters and colloids that they form on the surfaces of their pellets or of solid substrates can be regarded as molecularly homogeneous. The organic ligand shell itself is atomically inhomogeneous. However, because of its low electron density and the enhanced sensitivity of STM at low currents, it can be resolved by applying a very small tunneling current in the picoampere range.[23] The STM used did not offer this possibility because its signal-to-noise ratio was too low. Besides, the use of a low temperature STM is necessary to suppress the thermal movement of the ligands and therefore to have a chance to resolve the ligand shell, at least molecularly. For lack of atomic resolution, the STM images shown of the ligand-stabilized clusters and colloids can be correlated with their topography.

While the metal core and its surrounding ligand shell are monitored as a whole by AFM, the question if STM images of the clusters and colloids include their ligand shells is still not completely answered.[24] The presented results and measured particle sizes however, lead to the conclusion that the STM tip follows the outer contour of the ligand shells, which is confirmed by several publications.[1,2,6,25] In their role as adsorbates the ligands have to provide electronic states in the vicinity of the Fermi level of the metal core[26] or change its electronic structure[27,28] to be detected by STM. Nevertheless, a tunneling mechanism through the ligands is not yet defined.[24]

Discussion

Pellets of ligand-stabilized colloids and clusters

An essential requirement for the interpretation of STM and AFM images is a knowledge of the imaging mechanisms and the irregularities that could occur. The best-known effect is the microscopic enlargement of a spherical free-lying feature postulated by van Kempen and coworkers.[24,29] and by Magonov and Whangbo.[23] The position and the shape of the microscopically determined particle size distribution change dramatically with varying tip radii and tunneling distances, such that exact size determinations are not feasible with STM and AFM. The resulting microscopic dimensions have always to be compared with exact values determined by high resolution transmission electron microscopy (HRTEM), for example, to be able to interprete the STM and AFM images in a correct way. It has to be taken into account that the clusters and the colloids, in particular, have a size distribution determined by their synthesis.

In investigating the rough surface of a cluster or a colloid pellet, the particles lying free on the surface will be more enlarged than low-lying particles surrounded by other molecules. The scan of the tip over a pellet surface is schematically shown in Fig. 1. To improve clarity it is drawn in an exaggerated fashion.

Almost encapsulated low-lying particles may even be microscopically diminished because the scanning tip just reflects a part of the tops. The diminution results as the inverse effect on account of the microscopic enlargement of the neighbouring particles.

In most cases the effects of the microscopic enlargement and diminution are more enhanced when using STM because of the mostly larger tunneling distances compared with an AFM scanning in the contact mode. Nevertheless, both effects influence the shape of the microscopic particle size distribution enormously.

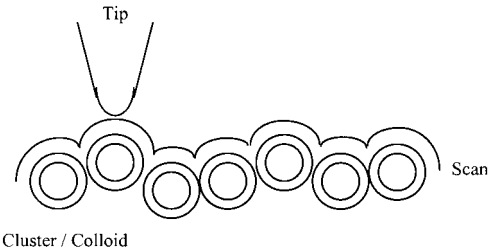

Fig. 1 Schematic scan profile of the STM or AFM tip above the surface of a cluster or colloid pellet, which is identical with a cross section of the microscopic image

Another effect can be mistaken for microscopic enlargement. If some particles lie very close together, STM or AFM may not be able to well-resolve them and thus monitors just one big feature. This mechanism is schematically seen in Fig. 2, which shows the cross section of the image of a cluster or colloid pellet as a result of low microscopic resolution. The described effect cannot be confirmed easily, either by AFM or STM themselves or by other physical methods. While remaining an assumption, it nevertheless gives an explanation for the mostly found broadening of the microscopic representation of spherical features.

Fig. 3 presents the STM (ARIS 4400, Burleigh Intruments) image of the pellet surface of a gold colloid Au_{Coll}[30,31] that is stabilized by the trisodium salt of triphenylphosphine trisulfonic acid (TPPTS). The densely but irregularly packed spherical features shown in Fig. 3 can each be identified as a

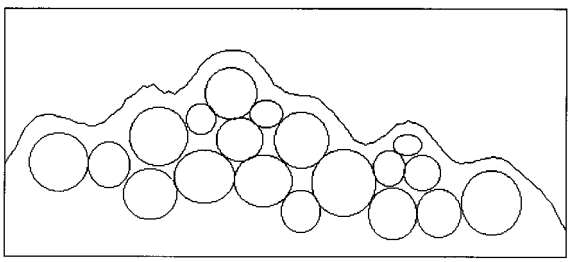

Fig. 2 Schematic cross section of the STM or AFM image of a pellet surface demonstrating the possible discrepancies between the real surface topography and the scan of the tip

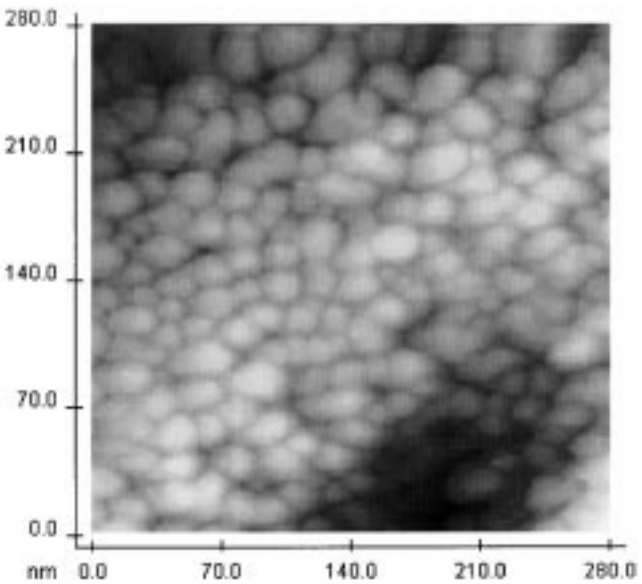

Fig. 3 STM image of the pellet surface of TPPTS-stabilized gold colloids Au_{Coll} taken at 3.7 nA and 30 mV[6]

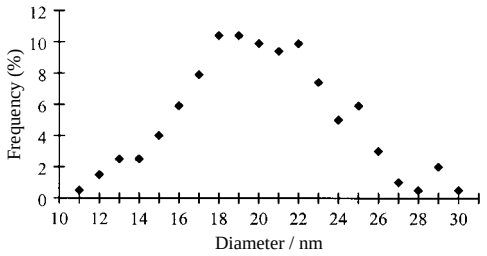

Fig. 4 Size distribution profile of TPPTS-stabilized gold colloids Au_{Coll} determined by STM of the pellet surface

colloid. The spherical shape of the gold colloids is already known from HRTEM.[32,33] Due to the high pressure during the synthesis of the pellets a nearly dense and homogeneous distribution of the colloids on the pellet surface can be supposed.

The particle size distribution profile is shown in Fig. 4. It is very broad but with the typical shape of a Gaussian distribution function it emphasizes the predominant presence of 18–22 nm large colloids as shown by the cross section in Fig. 5, which indicates a regular row of colloids.

Taking into account a single ligand layer with a thickness of 0.5–0.6 nm[1] or a double ligand layer with twice this thickness,[1,6,34,35] as occasionally observed on similar gold colloids by HRTEM, metal core diameters of 15–21 nm result. Comparable values were found for analogously synthesised gold colloids by HRTEM, showing core sizes of 18,[32] 16[33] or 13 nm,[7] as recently observed.

Supposing an enlarged monitoring of the colloids by STM, the real diameters will be smaller than 18–22 nm, a conclusion that is confirmed by the AFM images taken from the same pellet surface and discussed in the following.

An atomic force microscopic (ARIS 3300, Burleigh Instruments) characterized section of the pellet surface of the TPPTS-stabilized gold colloids Au_{Coll} is shown in Fig. 6. The particle diameters, whose Gaussian size distribution with a maximum at 10–12 nm is reflected in Fig. 7, are clearly smaller than those of 18–22 nm found by STM. As the same gold colloid pellet was investigated by both STM and AFM, the force microscopic results prove the strongly enlarged representation of the colloids by STM. In this case the enlargement even comprises several nanometers. Therefore, the colloids whose contour is drawn in Fig. 5 do not stick together so closely as is suggested by the cross section. Although AFM gives a more realistic representation of the colloids, it also tends to broaden their scanned contour. So the real diameter of the scanned gold colloids must be still less than 10–12 nm.

Monolayers of colloids and clusters

Before interpreting the AFM and STM images of the monolayers of ligand-stabilized colloids and clusters it is important to realize the scanning behaviour of the tip when following their surfaces.

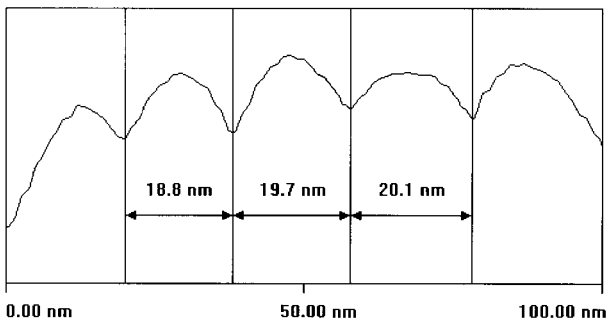

Fig. 5 Cross section of the STM image of the pellet surface of TPPTS-stabilized gold colloids Au_{Coll}

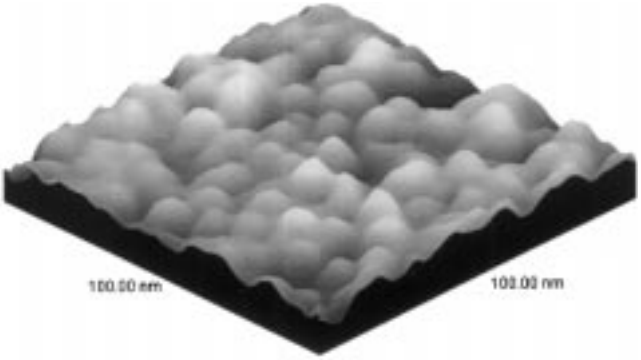

Fig. 6 AFM image of the pellet surface of TPPTS-stabilized gold colloids Au_{Coll}

If the particles of a monolayer lie horizontally side by side in a regular and closest packed manner on a substrate, as shown in Fig. 8, the movement of the tip reflects the very top of each cluster and colloid. In this special case the microscopic contour of each molecule agrees well with the real particle size. Then STM and AFM can be used quantitatively for size determinations. If the particles lie horizontally but loosely arranged on a substrate, with a separation smaller than the tip diameter, the tip is not able to get between the particles and to scan them separately. Instead, it follows the contour of their tops as in the case discussed before, but now the representation of each molecule is broadened. As shown in Fig. 9 the scan of the tip pretends a really dense arrangement. The

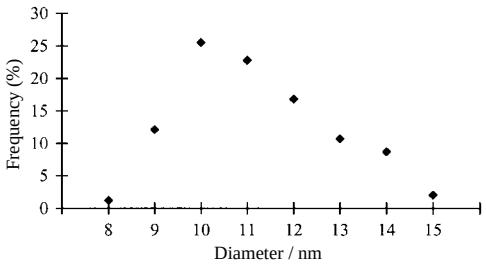

Fig. 7 Size distribution profile of TPPTS-stabilized gold colloids Au_{Coll} determined by AFM of the pellet surface

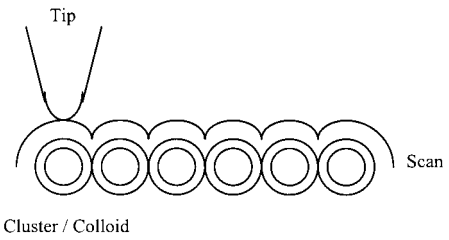

Fig. 8 Schematic scan profile of the STM or AFM tip above the surface of a closest packed row of clusters or colloids

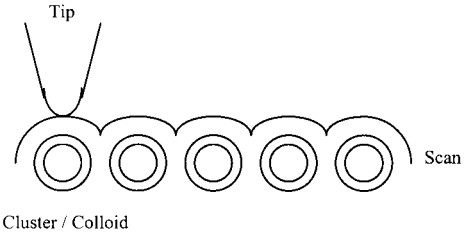

Fig. 9 Schematic scan profile of the STM or AFM tip above the surface of a loosely arranged row of clusters or colloids

microscopic molecule size results as the sum of the real particle diameter and the particle separation. Fig. 9 demonstrates clearly the diminished imaging of depressions as the inverse case to the broadened monitoring of free-lying features discussed by van Kempen and coworkers[24,29] and by Magonov and Whangbo.[23]

In consequence the position of the size distribution function of an investigated monolayer depends strongly on the separation of the molecules.

In opposition to the surfaces of cluster and colloid pellets, whose roughness is mainly determined by the roughness of the stamps of the pressing instrument, the monolayers of metal particles adopt the roughness of the substrate they adsorb onto. The smoother the surface of the substrate, the higher the quality of the self-assembled monolayer as concerns its order and density of packing.

Mica is well-suited to act as a substrate. It offers an atomically flat surface, which can easily be renewed by removing the topmost layers with an adhering tape. Because of its insulating character only AFM can be employed to characterize its surface. Some atomically resolved AFM images of mica surfaces have already been published.[36,37]

The preparation of the cluster and colloid monolayers using mica as a support is based on the principle described by Decher and coworkers[38,39] and by Ringsdorf and colleagues[40–42] to construct self-organized mono- and multilayers by insertion of multipolar polyelectrolytes. The polyelectrolyte polyethyleneimine (PEI),[7,10,38,41–44] adsorbed as a thin film, is well-suited to modify the mica sheet and to act as a spacer molecule for the subsequent adsorption of the ligand-stabilized clusters and colloids. While PEI exhibits mainly cationic groups in an acidic medium, it has very basic imine groups in a neutral medium, which are able to react with the acidic hydroxy groups[45,46] of the mica surface, as schematically shown in Fig. 10.[43]

Also based on an acid-base reaction, the imine groups of the adsorbed polymer react in a second adsorption and dipping process with the sulfonic acid groups of the clusters or colloids sitting at the outer surfaces of their ligand shells. The already described gold colloid Au_{Coll}, stabilized by the ligands TPPTS [$P(C_4H_6SO_3Na)_3$] and the smaller gold cluster $Au_{55}(Ph_2PC_4H_6SO_3Na)_{12}Cl_6$,[34,47] both soluble in water, are suitable candidates for the monolayer preparation. By exchanging their sodium ions for protons[48] they offer the required acidic groups. In the following, their protonated forms will be abbreviated as $Au_{Coll}SO_3H$ and $Au_{55}SO_3H$.

An AFM image of a monolayer of the gold colloids $Au_{Coll}SO_3H$, self-assembled on a mica surface that was first covered with PEI, can be seen in Fig. 11.[7,10] Similarly to the previously shown microscopic images of the colloid pellet, the AFM image in Fig. 11 monitors the colloids as hemispherical features in a quite dense but irregular arrangement. The broad size distribution, comprising sizes of 8–18 nm, presumably does not admit a regular order. Their mostly found diameters at 12–14 nm are a little bit larger than those at 10–12 nm determined by AFM when investigating their pellet surface.

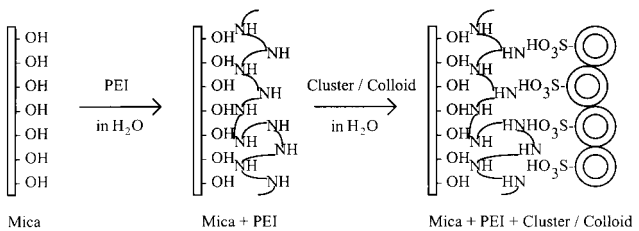

Fig. 10 Schematic self-organization of clusters and colloids on a layer of PEI and of PEI on mica. (Reproduced from ref. 43 with permission of Wiley-VCH Verlag GmbH)

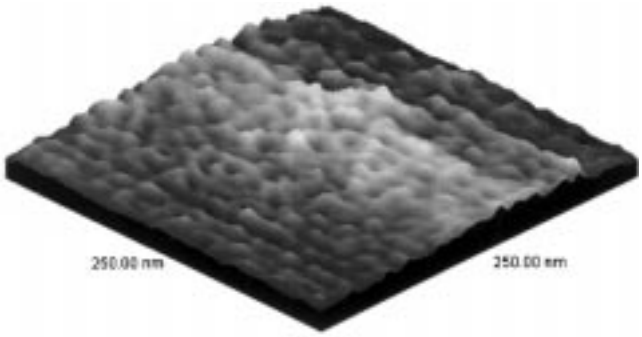

Fig. 11 AFM image of a monolayer of the gold colloids $Au_{Coll}SO_3H$ self-assembled on a layer of PEI adsorbed on mica; the concentrations of the aqueous solutions were 4×10^{-2} g L^{-1} for the colloid and 10^{-5} M for the polymer[7,10]. (Reproduced from ref. 7 with permission of HÜTHIG-Verlage)

Obviously, they are less densely packed in their monolayer than suggested by Fig. 11.

The AFM image of an analogously prepared monolayer of the gold clusters $Au_{55}SO_3H$ is given in Fig. 12.[43] The top of each cluster, whose spherical shape is already well-known from HRTEM[47,49] and explained by the full shell cluster model,[2,3,16,34] is reflected by one hemisphere measuring 2.4 ± 0.2 nm in diameter. This value corresponds well with the expected size of 2.3 nm, summing up the core diameter of 1.4 nm known from HRTEM[47] and the estimated thickness of the ligand layer at 0.4–0.5 nm, lying between the layer thickness of TPPTS of 0.5–0.6 nm[1] and that of the unsubstituted triphenylphosphine of 0.35 nm.[47] This agreement supports the closest packing of the clusters demonstrated by the microscopic picture in Fig. 12. In several sections the particles are regularly ordered and cluster rows are visible. Cross sections[43] prove the equidistance of the metal particles lying side by side as schematically seen in Fig. 8. The AFM image shown in Fig. 12 is filtered and flattened by a fast Fourier transformation (FFT), which emphasizes the periodic features of the topography.[21,50] By the loss of information about the aperiodic components, defects may be canceled. Nevertheless, defects are sparsely observed in the investigated monolayers indicating the topographic information.

A big disadvantage of the investigated monolayer systems is the formation of polymeric aggregates, seen as balls several tens of nanometers large. On the microscopic scale, monomer adsorption of the metal particles can occur between them. However, on the macroscopic scale the polymer balls prevent the adsorption of an even and close cluster and colloid monolayer.

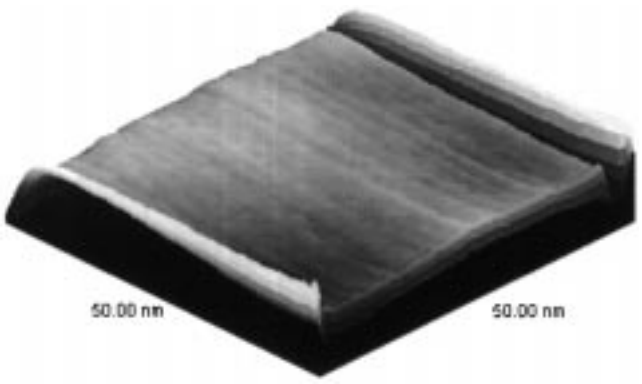

Fig. 12 AFM image of a monolayer of the gold clusters $Au_{55}SO_3H$ self-assembled on a layer of PEI adsorbed on mica; the concentrations of the aqueous solutions were 3×10^{-6} M for the cluster and 10^{-4} M for the polymer. (Reproduced from ref. 43 with permission of Wiley-VCH Verlag GmbH)

Gold is another material that is qualified to act as a substrate for the self-assembly of cluster and colloid monolayers. In this case aminothiols, strongly bound by their thiol function to the atomically flat gold surface in a monolayer,[19,51,52] are able to act as spacer molecules and to bind the metal particles in a monolayer. The amine groups of the self-organized spacer molecules react with the sulfonic acid functions of the cluster and colloid ligands in an acid-base reaction.[7]

Gold foils and gold films, sputtered on quartz glass at low temperatures, exhibit rough surfaces consisting of densely packed gold grains in the size range of 10–60 nm, as observed by STM and AFM and confirmed by other authors.[53–55] By tempering the gold substrates for 1 min at elevated temperatures[56] and then cooling them quickly down on a copper block, 200–900 nm large gold grains are formed, as observed by AFM in agreement with Chidsey *et al.*[54] On their flattened tops they exhibit Au(111) planes, as seen by the higher resolution STM. Because of their atomic flatness, the Au(111) regions especially are well-suited to form monolayers.

For the studies described in the following, 200 nm thick gold films, sputtered on thermally very stable tempax–quartz substrates, were taken.[57] To improve the adhesion of the gold on the quartz, each tempax substrate was first covered with a 2 nm thick chromium layer.[53,56,58]

In most cases the Au(111) surfaces on the grain tops lie one upon another, their step edges forming angles of 60° and 120° because of their trigonal structure.[56,59–61] Even equilateral triangles are observed.[56,60] In fact, atomically flat terraces with maximum sizes of nearly 200 nm can be prepared, separated from each other by their step edges, which often pass parallel.[37,55,56,59,60,62–64]

The aminothiols self-assemble from a 10^{-2} or 10^{-3} M ethanolic solution[19,65,66] on the tempered gold by a dipping process, in analogy to the already described monolayer preparation on mica. Dipping times of 24 h proved efficient to allow the self-organization of a nearly perfect thiol monolayer.[19,66]

In this study, 2-aminoethanethiol (AET) was chosen because its short length permits a tunneling current in the nanoampere range and a sufficient tunneling distance without being drastically damaged by the scanning tip, in accordance with STM lithography.[67] A slight deformation[68] of the 2-aminoethanethiols, in the *gauche* as well as in the *trans* conformation,[69] cannot be excluded. It was not possible to resolve the aminothiols molecularly or even atomically, because the STM used didn't offer low tunneling currents in the picoampere range, which are needed to detect the low electron density of the adsorbates.[23] Even the hole-structure, which was seen by STM by several authors[55,68,70–75] when characterizing alkanethiol monolayers on Au(111), was not observed. The only indication for the successful adsorption of the aminothiols is the observation of adsorbed metal particles after a second self-assembly step.

In contrast to the monolayer preparation on mica sheets the self-assembly of the TPPTS-stabilized gold colloids Au_{Coll} on 2-aminoethanethiol-modified Au(111) surfaces succeeds in a monomer and dense arrangement, as seen in the STM image in Fig. 13, only when very dilute colloid solutions are used.

The Gaussian size distribution function of the colloids exhibits a maximum at 13 nm, agreeing well with the colloid size of 10–12 nm found by AFM when investigating their pellet surface. Even provided that the real particles are some Ångstroms smaller than those observed by AFM, the colloids form an irregular, but dense packing on the gold surface, which is comparable with the drawing in Fig. 8.

Using higher colloid concentrations, like 4×10^{-2} g L^{-1} instead of 4×10^{-3} g L^{-1}, the colloids often adsorb as single lying molecules[6] or else they form large accumulations on the gold substrate, showing a dense and regular arrangement only within small sections.[6]

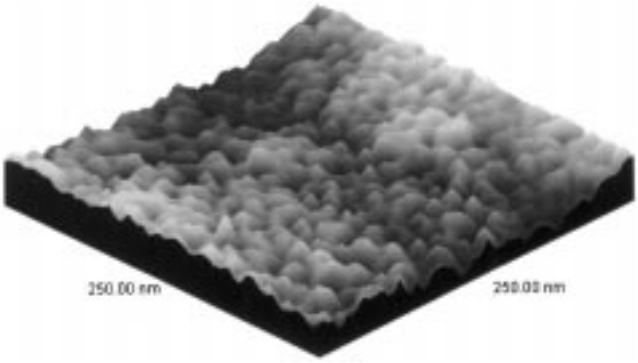

Fig. 13 STM image of a monolayer of the gold colloids $Au_{Coll}SO_3H$ self-assembled on a layer of AET adsorbed on Au(111) taken at 0.68 nA and 30 mV; the concentrations were 4×10^{-3} g L^{-1} for the colloids and 10^{-3} M for the thiol

Aggregation of the colloids, with loss of their ligand shells, may be responsible for their reduced reactivity at higher concentrations. This is indicated by their precipitation in solution, presumably induced by the dipped gold substrates as foreign bodies. The tendency to precipitate decreases with decreasing colloid concentrations, allowing monolayer preparation in very dilute solutions as demonstrated by Fig. 13.

More successful is the adsorption of monolayers of the gold cluster $Au_{55}SO_3H$. Its tendency to precipitate during the dipping process is less compared to that of the gold colloids. They also self-organize on aminothiol modified Au(111) surfaces, as the STM image in Fig. 14 demonstrates.[6,7,10] Microscopically a dense packing of the clusters, which sometimes even form rows, is observed. The mostly found cluster size of 4.5 nm is also twice the value of the more exact and already discussed size of 2.3 nm. So, a coverage rate of the gold clusters between 30–50% can be assumed. Scanning larger areas, even less densely packed monolayers of the gold clusters are visible, as shown in Fig. 15. For the first time the gaps between the clusters and the visible step edges of the Au(111) terraces indicate the monomer adsorption of the particles.

A complete coverage of the gold substrates with gold clusters could not be proven by STM because it was not possible

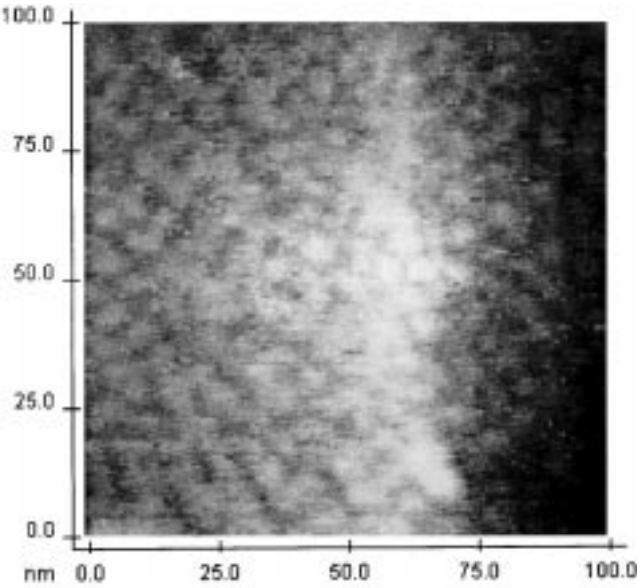

Fig. 14 STM image of a monolayer of the gold clusters $Au_{55}SO_3H$ self-assembled on a layer of AET adsorbed on Au(111) taken at 0.73 nA and 1.33 V; the concentrations were 3×10^{-6} g L^{-1} for the clusters and 10^{-2} M for the thiol[6,7,10]. (Reproduced from ref. 7 with permission of HÜTHIG-Verlage)

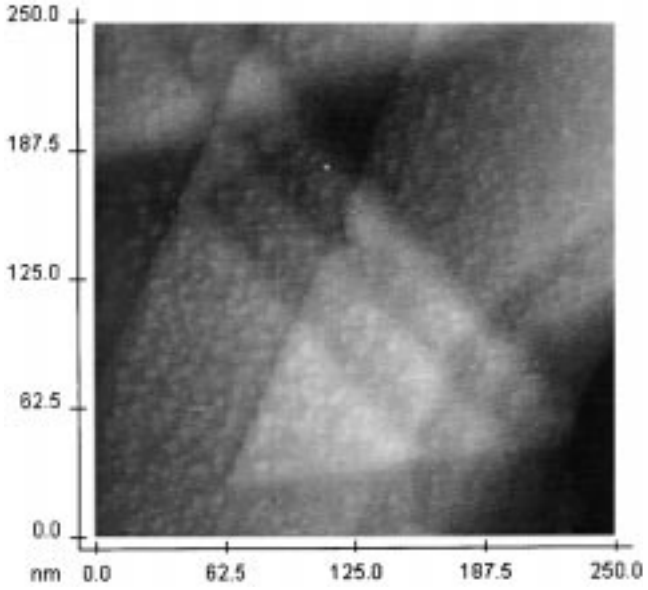

Fig. 15 STM image of a monolayer of the gold clusters $Au_{55}SO_3H$ self-assembled on a layer of AET adsorbed on Au(111) taken at 0.54 nA and 480 mV; the concentrations were 4×10^{-3} g L^{-1} for the clusters and 10^{-2} M for the thiol

to detect any of them on the grainy gold surface outside the Au(111) planes. Presumably the small corrugation wavelength and amplitude of a cluster layer surface are compensated by the higher roughness of the gold surface. This explanation is confirmed by the microscopic observation of the fourfold larger, analogously adsorbed gold colloids $Au_{Coll}SO_3H$ lying on grainy parts of the gold surfaces.

Even if the clusters also adsorb outside the Au(111) facets on the gold substrates, the deep gold grain boundaries hinder the formation of large, smooth and densely packed monolayers on the macroscopic scale. On the microscopic scale the size of an atomically flat Au(111) area on which regular and dense self-assembly of the metal particles can occur limits the dimensions of complete cluster and colloid monolayers.

Conclusions

Ligand-stabilized transition metal colloids and clusters are well-suited for the preparation of monolayer systems following the principle of self-assembly. This is demonstrated by the successful adsorption of the colloids $Au_{Coll}SO_3H$ and the clusters $Au_{55}SO_3H$ on polyethyeneimine-modified mica substrates on the one hand, and by the successful coverage of 2-aminoethanethiol-modified and tempered gold substrates with the clusters $Au_{55}SO_3H$ and $Pt_{309}SO_3H$ and partly with the colloids $Au_{Coll}SO_3H$ on the other hand. In all cases the surfaces of monolayers could be observed by AFM or STM. Although STM and AFM are only able to characterize the lateral electronic and topographic structure of surfaces, it can be assumed that the cluster and colloid adsorption is restricted to a monomer layer because of intermolecular repulsions. The same repulsive forces seem to be responsible for the sometimes observed loosely packed particle arrangements.

While the gold colloids are irregularly distributed within their monolayers the smaller gold clusters exhibit the start of order when they were self-assembled on mica as well as on gold. Their smaller size and size distribution more likely allows a regular particle arrangement rather than the larger colloids.

STM and AFM images of the same molecularly homogenous pellet surface of the gold colloids Au_{Coll} served as comparison patterns for the interpretation of the STM and AFM images of their self-assembled monolayers and also for the monolayers of the investigated clusters, because of their similar outer geometry. Both STM and AFM tend to image the spherical metal particles in a broadened manner, arising from a convolution between the scanning tip and the surface. The microscopic investigation of colloid pellets clearly showed that this effect is much more marked for STM than for AFM working in the contact mode. In spite of its poorer resolution, AFM is therefore better suited than STM to evaluate particle monolayers as concerns their density of packing, coverage rate and particle size distribution.

Acknowledgements

We gratefully acknowledge financial support of this work by the Deutsche Forschungsgemeinschaft. We also thank the Fond der Chemischen Industrie for their continuous support.

References

1 G. Schmid, *Chem. Rev.*, 1992, **92**, 1709.
2 G. Schmid, *Clusters and Colloids, From Theory to Application*, VCH, Weinheim, 1994.
3 G. Schmid, *Nachr. Chem. Tech. Lab.*, 1987, **35**, 249.
4 A. Gladun and A. B. Zorin, *Phys. Zeit*, 1992, **23**, 159.
5 U. Simon, G. Schön and G. Schmid, *Angew. Chem., Int. Ed. Engl.*, 1993, **32**, 250.
6 G. L. Hornyak, St. Peschel, Th. Sawitowski and G. Schmid, *Micron*, in press.
7 G. Schmid, St. Peschel and Th. Sawitowski, *Z. Anorg. Allg. Chem.*, 1997, **623**, 719.
8 E. Corcoran, *Spektr. Wiss.*, 1991, **1**, 76.
9 J. H. Fendler and F. C. Meldrum, *Adv. Mater.*, 1995, **7**, 607.
10 G. L. Hornyak, M. Kröll, R. Pugin, Th. Sawitowski, G. Schmid, J.-O. Bovin, G. Karrson, H. Hofmeister and S. Hopfe, *Chem. Eur. J.*, 1997, **3**, 1951.
11 G. Schön and U. Simon, *Colloid Polym. Sci.*, 1995, **273**, 101.
12 G. Nimtz and P. Marquardt, *J. Cryst. Growth*, 1988, **86**, 66.
13 R. Enderlein, *Mikroelektronik*, Spektrum Akademischer Verlag, Heidelberg, 1993.
14 K. K. Licharev and T. Claeson, *Spektr. Wiss.*, 1992, **8**, 62.
15 H. Grabert and M. H. Devoret, *Phys. Bl.*, 1994, **50**, 229.
16 G. Schmid, *Structure and Bonding*, 1985, **62**, 51.
17 G. Schmid, R. Pfeil, R. Boese, F. Bandermann, S. Meyer, G. H. M. Calis and J. W. A. van der Velden, *Chem. Ber.*, 1981, **114**, 3634.
18 G. Schmid and St. Peschel, unpublished results.
19 S. Buchholz, S., *GIT Fachz. Lab.*, 1993, **4**, 301.
20 *Scanning Tunneling Microscopy and Spectroscopy: Theory, Techniques and Applications*, ed. A. Bonnell, VCH, Weinheim, 1993.
21 *Surface Analysis with STM and AFM*, ed. S. N. Magonov and M.-H. Whangbo, VCH, Weinheim, 1996.
22 *Scanning Probe Microscopy and Spectroscopy: Methods and Applications*, ed. R. Wiesendanger, Cambridge University Press, Cambridge, UK, 1994.
23 S. N. Magonov and M.-H. Whangbo, *Adv. Mater.*, 1994, **6**, 355.
24 L. E. C. van de Leemput, J. W. Gerritsen, P. H. H. Rongen, R. T. M. Smokers, H.-A. Wierenga, H. van Kempen and G. Schmid, *J. Vac. Sci. Technol. B*, 1991, **9(2)**, 814.
25 C. Becker, Th. Fries, K. Wandelt, U. Kreibig and G. Schmid, *J. Vac. Sci. Technol. B*, 1991, **9(2)**, 810.
26 L. Koenders, *Phys. Zeit.*, 1993, **26**, 260.
27 D. Anselmetti, A. Baratoff, H.-J. Güntherodt, Ch. Gerber, B. Michel and H. Rohrer, *J. Vac. Sci. Technol. B*, 1994, **12**, 1677.
28 *Scanning Tunneling Microscopy I*, ed. H.-J. Güntherodt and R. Wiesendanger, Springer, Heidelberg, 1992.
29 H. A. Wieringa, C. C. Soethout, J. W. Gerritsen, L. E. C. van de Leemput, H. van Kempen and G. Schmid, *Adv. Mater.*, 1990, **2**, 482.
30 G. Schmid, A. Lehnert, U. Kreibig, Z. Adamczyk and P. Belouschek, *Z. Naturforsch., B*, 1990, **45**, 989.
31 J. Turkevich, P. C. Stevenson and J. Hillier, *Disc. Faraday Soc.*, 1951, **11**, 533.
32 G. Schmid and A. Lehnert, *Angew. Chem., Int. Ed. Engl.*, 1989, **28**, 780.
33 H. W. West, Thesis, University of Essen, 1995.
34 G. Schmid, *Endeavour, New Series*, 1990, **14**, 172.
35 J.-O. Bovin and J.-O. Malm, *Z. Phys. D*, 1991, **19**, 293.

36 J. Colchero, O. Marti, J. Mlynek, A. Humbert, C. R. Henry and C. Chapon, *J. Vac. Sci. Technol. B*, 1991, **9**, 794.
37 *Scanning Tunneling Microscopy II: Further Applications and Related Scanning Techniques*, ed. R. Wiesendanger and H. J. Güntherodt, Springer, Heidelberg, 1992.
38 G. Decher, *Nachr. Chem. Tech. Lab.*, 1993, **41**, 793.
39 G. Decher and J. D. Hong, *Ber. Bunsenges. Phys. Chem.*, 1991, **95**, 1430.
40 G. Mao, Y. Tsao, M. Tirrell, H. T. Davis, V. Hessel and H. Ringsdorf, *Langmuir*, 1995, **11**, 942.
41 L. F. Chi, R. R. Johnston, H. Ringsdorf, N. Kimizuka and T. Kunitake, *Thin Solid Films*, 1992, **210/211**, 111.
42 L. F. Chi, R. R. Johnston, H. Ringsdorf, N. Kimizuka and T. Kunitake, *Langmuir*, 1992, **8**, 1360.
43 G. Schmid and St. Peschel, *Angew. Chem., Int. Ed. Engl.*, 1995, **35**, 1442.
44 L. F. Chi, M. Anders, H. Fuchs, R. R. Johnston and H. Ringsdorf, *Science*, 1993, **259**, 213.
45 H. Yang, A. Kuperman, N. Coombs, S. Manicke-Afara and G. A. Ozin, *Nature* (*London*), 1996, **379**, 703.
46 D. W. Britt and V. Hlady, *J. Colloid Interface Sci.*, 1996, **178**, 775.
47 G. Schmid, N. Klein, L. Korste, U. Kreibig and D. Schönauer, *Polyhedron*, 1988, **7**, 605.
48 M. Harms, Thesis, University of Essen, 1992.
49 K. Fauth, U. Kreibig and G. Schmid, *Z. Phys. D*, 1991, **20**, 297.
50 P. K. Hansma, V. B. Elinger, O. Marti and C. E. Bracker, *Science*, 1988, **242**, 209.
51 A. Ulman, *Chem. Rev.*, 1996, **96**, 1533.
52 *An Introduction to Ultrathin Films: From Langmuir–Blodgett to Self-Assembly*, ed. A. Ulma, Academic Press, London, 1991.
53 R. G. Nuzzo, F. A. Fusco and D. L. Allara, *J. Am. Chem. Soc.*, 1987, **109**, 2358.
54 Ch. E. D. Chidsey, D. N. Loiacono, T. Sleator and S. Nakahara, *Surf. Sci.*, 1988, **200**, 45.
55 S. Buchholz, H. Fuchs and J. P. Rabe, *J. Vac. Sci. Technol. B*, 1991, **9**, 857.
56 W. Heiss, D. Lackey, J. K. Sass and K. H. Besocke, *J. Chem. Phys.*, 1991, **95**, 2193.
57 Given by G. Philipp, MPI Stuttgart.
58 D. N. Batchelder, S. D. Evans, T. L. Freeman, L. Häussling, H. Ringsdorf and H. Wolf, *J. Am. Chem. Soc.*, 1994, **116**, 1050.
59 J. V. Barth, H. Brune, G. Ertl and R. J. Behm, *Phys. Rev. B*, 1990, **42**, 9307.
60 J. A. DeRose, T. Thundat, L. A. Nagahara and S. M. Lindsay, *Surf. Sci.*, 1991, **256**, 102.
61 N. J. Tao and S. M. Lindsay, *J. Appl. Phys.*, 1991, **70**, 5141.
62 V. M. Hallmark, S. Chiang, J. F. Rabolt, J. D. Swalen and R. J. Wilson, *Phys. Rev. Lett.*, 1987, **59**, 2879.
63 M. P. Everson, R. C. Jaklevic and W. Shen, *J. Vac. Sci. Technol. A*, 1990, **8**, 3662.
64 D. J. Trevor and Ch. E. D. Chidsey, *J. Vac. Sci. Technol. B*, 1991, **9**, 964.
65 C. D. Bain, E. B. Troughton, Y.-T. Tao, J. Evall, G. M. Whitesides and R. G. Nuzzo, *J. Am. Chem. Soc.*, 1989, **111**, 321.
66 C. A. Widrig, C. A. Alves and M. D. Porter, *J. Am. Chem. Soc.*, 1991, **113**, 2805.
67 J. K. Schoer, C. B. Ross, R. M. Crooks, Th. S. Corbitt and M. J. Hampden-Smith, *Langmuir*, 1994, **10**, 615.
68 U. Dürig, O. Züger, B. Michel, L. Häussling and H. Ringsdorf, *Phys. Rev. B*, 1993, **48**, 1711.
69 L. S. Wong, V. L. Vilker, W. T. Yap and V. Reipa, *Langmuir*, 1995, **11**, 4818.
70 J. P. Bucher, L. Sautesson and K. Kern, *Appl. Phys. A*, 1994, **59**, 135.
71 S. J. Stranick, M. M. Kamna, K. R. Krom, A. N. Parikh, D. L. Allara and P. S. Weiss, *J. Vac. Sci. Technol. B*, 1994, **12**, 2004.
72 R. G. Nuzzo, B. R. Zegarski and L. H. Dubois, *J. Am. Chem. Soc.*, 1987, **109**, 733.
73 D. Anselmetti, Ch. Gerber, B. Michel, H. Wolf, H. J. Güntherodtm and H. Rohrer, *Europhys. Lett.*, 1993, **23**, 421.
74 L. Häußling, B. Michel, H. Ringsdorf and H. Rohrer, *Angew. Chem.*, 1991, **103**, 568.
75 C. Schönenberger, J. A. M. Sondag-Huethorst, J. Jorritsma and L. G. J. Fokkink, *Langmuir*, 1994, **10**, 611.

Received in Montpellier, France, 2nd October 1997;
Paper 7/09222I